Atmospheric dispersion using a Lagrangian stochastic approach: Application to an idealized urban area under neutral and stable meteorological conditions

Meïssam Louisa Bahlali, Eric Dupont, Bertrand Carissimo

▶ **To cite this version:**

Meïssam Louisa Bahlali, Eric Dupont, Bertrand Carissimo. Atmospheric dispersion using a Lagrangian stochastic approach: Application to an idealized urban area under neutral and stable meteorological conditions. Journal of Wind Engineering and Industrial Aerodynamics, 2019, 193, pp.103976. 10.1016/j.jweia.2019.103976 . hal-02898281

HAL Id: hal-02898281
https://enpc.hal.science/hal-02898281

Submitted on 20 Jul 2022

HAL is a multi-disciplinary open access archive for the deposit and dissemination of scientific research documents, whether they are published or not. The documents may come from teaching and research institutions in France or abroad, or from public or private research centers.

L'archive ouverte pluridisciplinaire **HAL**, est destinée au dépôt et à la diffusion de documents scientifiques de niveau recherche, publiés ou non, émanant des établissements d'enseignement et de recherche français ou étrangers, des laboratoires publics ou privés.

Distributed under a Creative Commons Attribution - NonCommercial 4.0 International License

Version of Record: https://www.sciencedirect.com/science/article/pii/S0167610519305768
Manuscript_0fae4fba608e17d6ca5963c27b6024fa

Atmospheric dispersion using a Lagrangian stochastic approach: application to an idealized urban area under neutral and stable meteorological conditions

Meïssam L. Bahlali[a,b,*], Eric Dupont[b], Bertrand Carissimo[b]

[a] *Department of Civil and Environmental Engineering, Imperial College London, London, UK*
[b] *CEREA, Joint laboratory Ecole des Ponts ParisTech/EDF R&D, 6 quai Watier, 78401 Chatou Cedex, France*

Abstract

We present an adaptation of the Lagrangian stochastic dispersion model of the computational fluid dynamics (CFD) open source code *Code_Saturne* to simulate atmospheric dispersion of pollutants in complex urban geometries or around industrial plants. The wind is modeled within the same code with an Eulerian RANS (Reynolds-averaged Navier-Stokes equations) approach and thus involves the solution for the ensemble-mean velocity field and turbulent moments, using eddy viscosity or Reynolds stress turbulence models adapted to the atmosphere and complex geometries. The Lagrangian stochastic model used for the dispersion of the particles within this flow field is the simplified Langevin model, which pertains to the approaches referred to as PDF (Probability Density Function) methods. This formulation of model has not been widely used in atmospheric applications, despite interesting theoretical and computational benefits. Therefore, its usage must be validated on different atmospheric cases. In this paper, we present the validation of the model with a field experiment, considering atmospheric stratification and buildings: the MUST (Mock Urban Setting Test) campaign, conducted in Utah's desert, USA.

Keywords: Atmospheric dispersion, Lagrangian models, Eulerian models, Wind flow modeling, MUST experiment

1. Introduction

An atmospheric dispersion model is a tool that can be used to simulate the atmospheric phenomena involved in the turbulent pollutant dispersion process. The differences between the many existing models to date are mainly in terms of the number of atmospheric processes considered, their degree of complexity, their field of application and, in particular, the methods used to solve the equations governing them. We can distinguish mainly three types of models:

- Gaussian models, based on the analytical resolution of the so-called advection-diffusion equation (on a scalar corresponding to the concentration of pollutant) coupled with semi-empirical parameterizations of the main physical phenomena;

*Corresponding author: meissambahlali@gmail.com
This research was done while M. L. Bahlali was a Ph.D. student at CEREA, in 2015-2018.

© 2019 published by Elsevier. This manuscript is made available under the CC BY NC user license
https://creativecommons.org/licenses/by-nc/4.0/

- Eulerian models, based on the resolution of the discretized advection-diffusion equation in time and space on a mesh;

- Lagrangian models, based on the computation of particle trajectories.

Eulerian models, when used through Computational Fluid Dynamics (CFD) methods, rely on the resolution of the advection-diffusion equation of a scalar on a mesh. This equation implies the knowledge of the velocity and turbulent fields. Therefore, the first step is the resolution of the Eulerian Navier-Stokes momentum equation, in order to compute the flow field over which the dispersion will be calculated. Generally, the resolution of the Navier-Stokes momentum and scalar transport equations are carried out within the same model. This therefore supposes to have a model that provides a solution for the dynamical fields of high enough quality, since it strongly influences the solution obtained for the concentration field calculated through the advection-diffusion equation. In particular, this highlights the crucial importance of a correct modeling of flow turbulence. This topic has been addressed in various papers as atmospheric simulations using CFD have been increasingly used in the past few decades (Franke et al., 2004; Blocken, 2014), especially at local scale (with, for instance, studies of wind flow patterns at pedestrian level around buildings, see Yoshie et al. (2007); Mochida et al. (2008); Tominaga et al. (2008); Blocken and Stathopoulos (2013)).

On the other hand, Lagrangian models consist of calculating and following the trajectories of particles in a turbulent flow. Thus, the frame of reference is not fixed but follows the cloud described by a large number of particles emitted into the atmosphere. For each of these particles, a stochastic differential equation of a Langevin type is written on their velocity. By integrating over time, we are thus able to get the position of each and then deduce the concentration field over the computational domain. The main strength of Lagrangian models is that they treat convection without any approximation. In particular, they can treat without approximation local source terms when they are provided as known expressions of the variables associated with the particles, such as chemical source terms (Minier, 2015). Also, Lagrangian models are grid-free, which makes them accurate to capture the different turbulent structures in a statistical sense and avoid numerical diffusion problems that can be encountered within Eulerian models – especially near the source. However, one must keep in mind that they usually still depend on a grid in two ways:

- the stochastic differential equation that governs the velocity evolution of the particles usually involves fluid mean quantities that are in practice provided by a grid-based meteorological pre-processor or a CFD calculation;

- the concept of 'concentration' is by definition mesh-based.

Both CFD Eulerian and Lagrangian models are well-suited for atmospheric dispersion studies in urban neighborhoods or around industrial plants, in the sense that they are capable of capturing the complex interactions between the air flow and the buildings for different meteorological conditions. However, these two types of models have often been

compared ignoring the level of turbulence closure used for each. Loosely speaking, a common belief is that 'Eulerian models do not work well near the source'. In reality, a more correct affirmation would be: 'Eulerian models that are based on a gradient-diffusion hypothesis do not work well near the source', since this region corresponds to the short-time limit where the fully diffusive regime has not been reached yet (Taylor, 1921). In fact, in the atmospheric dispersion field, Lagrangian models are commonly referred to models simulating the particle **velocities** as stochastic diffusion processes, which by construction makes them second-order. On the other hand, a Lagrangian model simulating the **positions** as stochastic diffusion processes is equivalent to an Eulerian model using a gradient-diffusion hypothesis. More details can be found on that subject in Minier (2016). To sum up, the Eulerian/Lagrangian comparisons should not be about the approaches in themselves but rather about the level of closure that is considered. Throughout this paper, we will be coming back on this point of significant importance when it comes to rigorously comparing the accuracy of the results given by both approaches.

In the past few years, the constantly increasing computing power has enabled (and above all made easier) the use of Lagrangian stochastic methods for atmospheric purposes – see for example Franzese (2003), Stohl et al. (2005), Cassiani et al. (2005a,b), Bernardin et al. (2009), Alessandrini and Ferrero (2009), Tinarelli et al. (2013), etc. For our work, a simulation tool using a Lagrangian PDF (Probability Density Function) to carry out pollutant dispersion studies has been developed in the three-dimensional CFD code *Code_Saturne* (`http://code-saturne.org/`, see Archambeau et al. (2004) for more details). It has been validated on simple academic cases and shown to satisfactorily respect the well-mixed condition (see Bahlali et al. (2018a,b)). This paper is concerned with validating the model in real conditions by studying continuous point source dispersion of a non-reactive pollutant in an idealized urban area, as such a case is typical of industrial emissions or an accidental release.

The present work will focus on the Mock Urban Setting Test (MUST) campaign, which has been widely studied in the literature. For previous numerical simulations of the experiment, the reader may for example refer to Hanna et al. (2004), Camelli et al. (2005), Donnelly et al. (2009), Antonioni et al. (2012), Kumar et al. (2015). Comparisons between different modeling systems have also been studied: Santiago et al. (2010) and Dejoan et al. (2010) compared large-eddy simulations (LES) to Reynolds-averaged Navier-Stokes (RANS) computations, and Castelli et al. (2017) performed comparisons between different atmospheric Eulerian and Lagrangian modeling approaches. Experimental comparisons have been conducted as well: Leitl et al. (2007) worked on the Hamburg wind tunnel experiment, and Yee et al. (2006) compared experimental wind-tunnel and water-channel simulations.

In the CFD code *Code_Saturne*, previous numerical simulations of the MUST campaign have also already been performed by Milliez and Carissimo (2007, 2008) and used an Eulerian $k-\epsilon$ model of turbulent dispersion. The present work aims at studying the same cases using the Lagrangian stochastic model. The objective is twofold:

- first, we would like to assess the accuracy of the results provided by the Lagrangian model for this specific industrial application;

- second, we would like, in the same CFD simulations, to compare the Lagrangian results to the ones obtained with several Eulerian turbulence models, and above all explain the differences to provide a better understanding of the different modeling options.

A specificity of this work is that the wind is modeled *within the same code* as the dispersion, with an Eulerian RANS approach. It thus involves the solution for the ensemble-mean velocity field and turbulent moments, using $k-\epsilon$ or second-moment $R_{ij}-\epsilon$ turbulence closures adapted to the atmosphere and complex geometries. In the aforementioned notations, k is the turbulent kinetic energy (TKE), ϵ the turbulent dissipation rate and R_{ij} the Reynolds stress tensor. Note that Milliez and Carissimo (2007, 2008) only simulated the wind dynamical mean fields using a $k-\epsilon$ model. Therefore, in addition to the Lagrangian results, this paper will also expose new results on the Eulerian approach through the use of the second-order $R_{ij}-\epsilon$ model for the wind mean quantities.

This paper will be organized as follows. First, both the Eulerian and Lagrangian model equations used in this work will be introduced. Second, the experiment characteristics will be exposed and the two cases chosen for this study will be described. Finally, results for both these cases will be shown and the different modeling approaches will be discussed.

2. Model equations

The methodology for atmospheric dispersion calculations in *Code_Saturne* consists of two simulations:

- the first simulation solves the mean Navier-Stokes equations for the flow field;

- the second simulation restarts from the previous frozen flow field (velocity, turbulence and temperature) and computes the dispersion.

In the following subsections, the different modeling options in Eulerian and Lagrangian approaches are presented.

2.1. The Eulerian approach

Eulerian models, as explained in the introduction, are based on the resolution of the mean advection-diffusion equation of a given Reynolds-averaged scalar $\langle c \rangle$ through its discretization in time and space on a mesh. This equation is written as:

$$\frac{\partial \langle c \rangle}{\partial t} + \langle U_{f,j} \rangle \frac{\partial \langle c \rangle}{\partial x_j} = \frac{\partial}{\partial x_j} \left(D \frac{\partial \langle c \rangle}{\partial x_j} - \langle U'_{f,j} c' \rangle \right) + \langle S \rangle + \langle R \rangle \ , \tag{1}$$

where $U_{f,j}$ is the fluid velocity along the j axis, D the molecular diffusivity, S and R respectively the source and reactive terms. Also, the notation $\langle\rangle$ stands for Reynolds average and $'$ its deviation part.

This equation involves the unknown term $\langle U'_{f,j}c'\rangle$. For practical applications, two main families of closures are considered:

- eddy diffusivity models, which directly provide a local expression for $\langle U'_{f,j}c'\rangle$;
- second-order models, which consist of a complete transport of the turbulent scalar fluxes $\langle U'_{f,j}c'\rangle$.

Eddy diffusivity models are widely used in the atmospheric dispersion literature, usually through the following simple gradient-diffusion hypothesis:

$$\langle U'_{f,j}c'\rangle = -D_t \frac{\partial\langle c\rangle}{\partial x_j} \ , \tag{2}$$

where $D_t = \nu_t/Sc_t$, Sc_t being the turbulent Schmidt number, usually ranging between 0.7 and 1 for air.

In this expression, $\nu_t = C_\mu k^2/\epsilon$ is the fluid turbulent viscosity, $k = (1/2)\ R_{ii}$ where by definition $R_{ij} = \langle U'_{f,i}U'_{f,j}\rangle$. In $k-\epsilon$ models, R_{ij} is constructed as follows:

$$R_{ij} = (2/3)\ k - 2\ \nu_t\ S_{ij} \tag{3}$$

where $S_{ij} = (\partial U'_{f,i}/\partial x_j + \partial U'_{f,j}/dx_i)/2$, so that R_{ij} is symmetric and $\mathrm{Tr}(R_{ij}) = 2k$.

An important point to recall here is that if a turbulent-viscosity model is used for the resolution of the mean dynamical fields, then obviously, closure of $\langle U'_{f,j}c'\rangle$ will be performed through a 'turbulent-diffusivity' model. On the other hand, one can use a second-order $R_{ij}-\epsilon$ model to compute the mean dynamical fields and still use a turbulent-diffusivity model for the turbulent scalar fluxes closure (*i.e.*, here, the model of Eq. (2)). The present work will provide new elements on that topic, by comparing, using either a $k-\epsilon$ or a $R_{ij}-\epsilon$ model to compute the mean dynamical fields, the results obtained through a turbulent-diffusivity model for the scalar dispersion. As for second-order scalar fluctuations models for meteorological applications, they are in fact still an open and difficult research problem, and the subject of further investigations.

2.2. The Lagrangian approach

Let $\mathbf{X}_p$ be the position of a particle included in the air flow and $\mathbf{U}_p$ its velocity. Both variables are driven by the following system:

$$dX_{p,i} = U_{p,i}(t)dt \ , \tag{4a}$$

$$dU_{p,i} = -\frac{1}{\rho}\frac{\partial\langle P\rangle}{\partial x_i}dt + (\langle U_{p,i}\rangle - \langle U_{f,i}\rangle)\frac{\partial\langle U_{f,i}\rangle}{\partial x_i}dt - \frac{U_{p,i}-\langle U_{f,i}\rangle}{T_L}dt + \sqrt{C_0\epsilon}dW_j \ , \tag{4b}$$

where dW_j are independent Wiener processes. Briefly speaking, a Wiener process is a Gaussian process with independent increments of zero mean and with a variance equal to dt (more details can be found in Gardiner (1985); Öttinger (1996)). Also, $T_L = \frac{1}{\frac{1}{2}+\frac{3}{4}C_0}\frac{k}{\epsilon}$ is the Lagrangian integral timescale and C_0 is a constant given by Kolmogorov's theory.

In Eq. (4b), the sum of the first, second and third terms on the right-hand-side is known as the drift term. More precisely, the drift term is the sum of a mean component (the mean pressure gradient $-\frac{1}{\rho}\frac{\partial\langle P\rangle}{\partial x_i}dt$ and the term accounting for the crossing-trajectory effect $\langle U_{p,i}\rangle - \langle U_{f,i}\rangle)\frac{\partial\langle U_{f,i}\rangle}{\partial x_i}dt$, more detailed in the following paragraph) and a fluctuating component (the return-to-equilibrium term $-\frac{U_{p,i}-\langle U_{f,i}\rangle}{T_L}dt$). On the other hand, the fourth term on the right-hand-side of Eq. (4b) is known as the diffusion term and is defined following Kolmogorov's similarity theory.

The stochastic differential equation governing the evolution of $\mathbf{U}_p$ is a model inspired by the two-phase flow formulation of Minier and Peirano (2001) and the Simplified Langevin Model (SLM) of Pope (2000) – it actually stands between the two of them, the difference lying in the $(\langle U_{p,i}\rangle - \langle U_{f,i}\rangle)\frac{\partial\langle U_{f,i}\rangle}{\partial x_i}dt$ term. The formulation with this term makes sense since even though we are dealing with fluid particles (putting us in the single-phase flow situation), particles dispersing from a point source can be seen as a subset of the whole simulated flow. Therefore, in each cell of the computational domain, their mean velocity has no reason to be equal to the fluid velocity, hence the non-null production term on the second term of the right-hand-side of Eq. (4b). In fact, for a better understanding, let us assume that the whole flow is represented by particles uniformly distributed in the domain and affect a scalar α to each of them:

$$\begin{cases} \alpha = 1 \text{ if the particle comes from the source;} \\ \alpha = 0 \text{ if it does not come from the source.} \end{cases}$$

Therefore, the condition that the mean particle velocity field needs to observe is: $\mathbf{div}(\alpha\langle\mathbf{U}_p\rangle) = \mathbf{0}$, which is a completely different condition than the one the fluid velocity field has to meet, *i.e.*, $\mathbf{div}(\langle\mathbf{U}_f\rangle) = \mathbf{0}$.

Loosely speaking, this formulation stands in a philosophical line that is close to the LRR-IP (Launder, Reece, Rodi - Isotropization of Production) model of Pope (2000), except that the production term here is related to the mean particle velocity instead of the instantaneous one. This production term actually makes significant physical sense, since it adds more anisotropy to the dispersion of the particles. Furthermore, if one studies the limiting case of particles modeling the whole flow (*i.e.*, the 'fluid limit'), then it yields $\langle U_{p,i}\rangle = \langle U_{f,i}\rangle$ and the SLM is retrieved. More precisely, Bahlali et al. (2018b) have shown that the SLM fully respects the well-mixed criterion (as defined in Thomson (1987)) and that it is completely consistent with a second-order $R_{ij}-\epsilon$ (Rotta) turbulence model for the fluid phase. Both these conditions are in fact essential for any Lagrangian stochastic model of a Langevin type to be regarded as acceptable (see Minier et al. (2014)). In conclusion, the model defined in Eq. (4), since it relaxes to the SLM for the fluid limit, is well-mixed

and able to reproduce transport equations for the first two moments of the velocity field: it can thus reasonably be used to simulate point source dispersion in non-homogeneous flows such as the one studied in this work. However, one must keep in mind that this model has been developed for neutral conditions. It is possible to use it also for buoyancy-driven flows, as we did in the present work, but some improvements can be made for these cases and are the subject of further investigations (cf. conclusion).

It should be noted that this Lagrangian model alone does not take into account molecular diffusion. Indeed, if a scalar c is added to the state vector associated with each particle, then: $dc/dt = 0$ (conservative particles are studied, with a constant concentration along their trajectories). In order to represent the molecular diffusion phenomenon, a so-called 'micro-mixing model' can be used (see, for example, Villermaux and Devillon (1972); Pope (2000); Sawford (2004); Luhar and Sawford (2005); Amicarelli et al. (2012); Cassiani et al. (2015)). This type of model is often used in the case of reactive pollutants, since in this context molecular diffusion plays an important role. In the case of high Reynolds numbers, molecular diffusion does not affect the concentration mean (Pope, 1998), and is therefore generally neglected compared to turbulent diffusion.

3. The Mock Urban Setting Test experiment

3.1. Description of the site

The experimental program this paper focuses on is the Mock Urban Setting Test campaign, conducted in Utah's desert, USA, by the US Defense Threat Reduction Agency (DTRA). It consists of the release of a pollutant in an idealized urban environment represented by several rows of containers. The details of the experiment as well as the results are described in Biltoft (2001) and Yee and Biltoft (2004).

It is worth noting that pollutant dispersion simulations in urban geometries using CFD have been widely studied in the past few years, for instance within street canyons (Tominaga and Stathopoulos, 2011; Salim et al., 2011) or around high-rise buildings (Yoshie et al., 2011). In this work, the objective is to reproduce some of the simulations of the MUST campaign that have already been performed in the past by Milliez and Carissimo (2007, 2008) in *Mercure* (former name of the atmospheric module of *Code_Saturne*), but completing them with new results using the Lagrangian stochastic model previously introduced and the second-order $R_{ij} - \epsilon$ model for the fluid phase computation. Milliez and Carissimo (2007) described in detail the characteristics of the campaign, which are summarized below:

- 63 emissions of a neutral gas (propylene C_3H_6), among which 58 are continuous and 5 are puff releases;
- flat terrain with some bushes from 50 cm to 1 m high;
- presence of obstacles through a regular alignment of containers of dimensions 12.2 m (length) $\times$ 2.42 m (width) $\times$ 2.54 m (height);

Figure 1: Some views of the MUST experiment (after Milliez (2006)).

- different wind conditions through varying angles of incidence, wind velocities, turbulence, temperature, stability conditions;
- different release heights: 0.15 m, 1.3 m, 1.8 m, 2.6 m and 5.2 m.

Figure 1 shows two photos of the MUST experiment. The regular alignment of the containers is supposed to represent an idealized city and the objective of the experiment is to observe the point source dispersion of the propylene continuously released in this environment. We are interested in checking how the Lagrangian model behaves in the presence of obstacles in a real situation. Indeed, when assessing the respect of the well-mixed criterion for the SLM, Bahlali et al. (2018b) studied the case of a non-homogeneous turbulent flow around an obstacle within a boundary layer and observed notable differences in the behavior of the particles depending on the turbulence model that was used to compute the fluid phase.

The experimental devices used in the campaign are illustrated in Figure 2. Wind and temperature measurements were carried out using sonic anemometers (30-m mast S just upstream of the canopy, 32-m central tower T and 8-m masts A, B, C and D inside the canopy). As for pollutant concentrations, they were measured by photoionization detectors (PIDs), positioned on four horizontal lines (*'line 1, 2, 3, 4'* in Figure 2). These four lines were located at height 1.6 m. PIDs were also placed at 6 levels on the masts A, B, C, D and at 8 levels on the tower T.

Finally, it should be noted that the tracer releases occured at dusk or dawn, thus under meteorological conditions ranging from stable to neutral. The duration of each release was 15 min and for the analysis of the results, periods of 200 s were extracted by Yee and Biltoft (2004). These periods were indeed quasi-steady in terms of wind speed and direction and also remained greater than the plume travel time.

3.2. Description of the cases studied

As previously mentioned, the MUST experiment consisted of 63 tracer releases and in the work of Milliez and Carissimo (2007, 2008), twenty cases were simulated. In the present

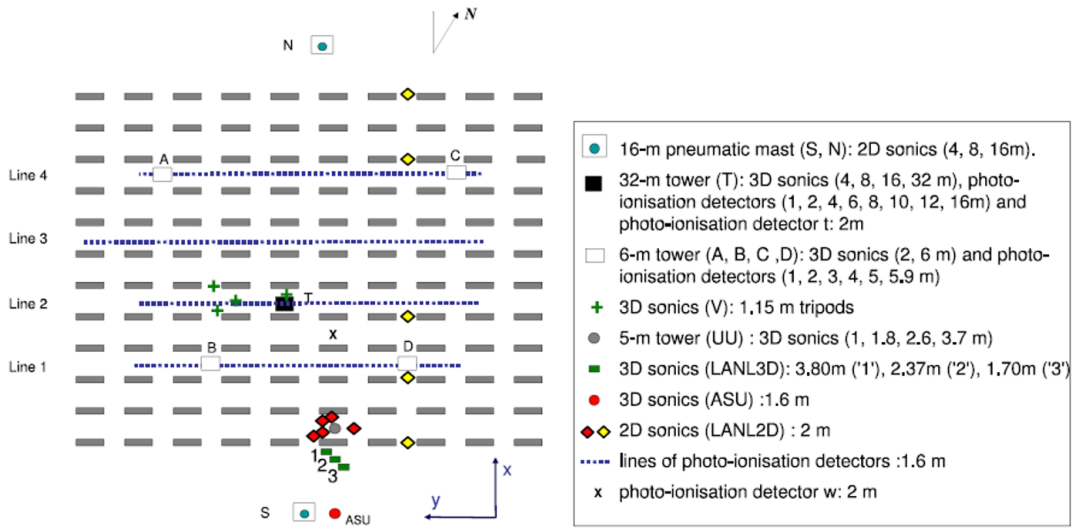

Figure 2: Schematic diagram of the MUST experiment and location of the experimental devices (after Milliez and Carissimo (2008)).

Case	α_4 (deg)	S_4 (m.s $^{-1}$)	k_4 (m^2.s $^{-2}$)	L (m)	Q (L.min^{-1})	Source location	z_s (m)
2681829	-41	7.93	4.263	28000	225	29	1.8
2692157	43	2.98	0.510	130	225	36	2.6

Table 1: Characteristics of the two selected trials: S_4 and α_4 are respectively the mean wind horizontal speed and direction at the 4-m level of mast S, k_4 is the turbulent kinetic energy and L the Monin-Obukhov length at the 4-m level of tower T, Q is the tracer release rate at the source, 'Source location' is the position of the source and z_s is the height of the source (after Milliez and Carissimo (2007)).

paper, trials 2681829 and 2092157 are studied, respectively corresponding to situations of neutral and stable atmospheres. The characteristics of these trials are summarized in Table 1, and the characteristics of all cases can be found in Milliez and Carissimo (2007).

More precisely, the MUST simulations made in different meteorological conditions by Milliez and Carissimo (2007) have been reused. These simulations only used the Eulerian approach with a $k-\epsilon$ turbulence closure. In this paper, new $R_{ij}-\epsilon$ Eulerian and Lagrangian dispersion simulations are provided within the same calculations so that they can be compared with the same Eulerian dynamical field, including the stratification effects. To take into account these effects, the code solves for potential temperature, as fully explained in Milliez and Carissimo (2007)).

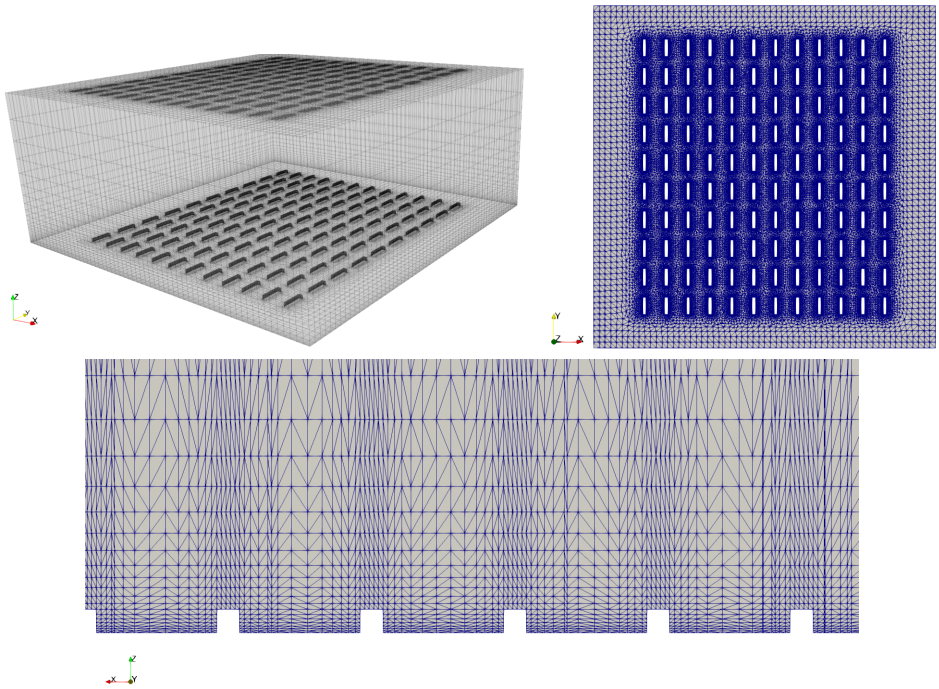

Figure 3: Mesh of the computational domain. From left to right and top to bottom: general view, horizontal cross-section, vertical cross-section.

4. Numerical simulations

In this section, the methodology and results of the numerical simulations of trials 2681829 and 2692157 in *Code_Saturne* are presented.

4.1. Simulation domain and mesh

The simulation domain is of dimensions 240 m (North-South) × 240 m (East-West) × 100 m (vertical direction). The corresponding mesh is displayed in Figure 3. It is refined near the ground and the obstacles, the horizontal resolution varying from 4 m to 0.6 m. The vertical resolution of the mesh increases gradually from 0.2 m near the ground until it reaches 4 m at the top of the domain. In total, the mesh contains 1 426 010 cells.

4.2. Numerical setup

4.2.1. Fluid phase

For the flow, the models $k-\epsilon$ et $R_{ij}-\epsilon$ (with simple gradient-diffusion hypothesis for the scalars) are used and will be further compared. The imposed boundary conditions are as follows:

- Inlet condition of Dirichlet type, with dynamical profiles derived from experimental measurements. Indeed, it has been shown in Milliez and Carissimo (2007) that

the use of analytical profiles in equilibrium can induce an underestimation of turbulence. They found better results using experimental profiles (when available), which is why we have chosen to follow the same road. More precisely, the TKE profiles are estimated from the available measurements and then the turbulent dissipation rate profiles are deduced from the relations from Monin-Obukhov theory as given in Duynkerke (1988) and reused in Milliez and Carissimo (2007):

$$k = \frac{{u_L}^2}{\sqrt{C_\mu}}, \tag{5a}$$

$$\epsilon = \frac{{u_L}^3}{\kappa}\left(\frac{1}{z} + \frac{4}{L}\right), \tag{5b}$$

where u_L is the local stress equal to $u_*(1-z/h)$ where h is the height of the boundary layer (Stull, 1988) and u_* the surface stress. Also, κ is the von Karman constant and L is the Obukhov length.

In the case of the $R_{ij}-\epsilon$ model, the R_{ij} tensor at the boundary is given as follows: the diagonal terms are constructed isotropically from the turbulent kinetic energy and the other terms are taken as zero. These are reasonable hypotheses that can be expected in operational use (and similar for both $k-\epsilon$ and $R_{ij}-\epsilon$ models). We have verified elsewhere that the model rapidly adjusts to a more realistic R_{ij} tensor, well before reaching the obstacles.

- Outlet condition: free outflow.
- Ground and containers: rough wall, with a roughness length of 0.04 m. A logarithmic wall function is used. A Dirichlet condition is applied for k, such that $k = u_*^2/\sqrt{C_\mu}$ except in the viscous sub-layer where $k = 0$. A Neumann condition is applied for ϵ, such that $\epsilon = u_*^3/(\kappa z)$, except in the viscous sublayer where a zero-flux is imposed.

4.2.2. Dispersed phase

With the Eulerian approach, the pollutant is injected through a scalar source term. At the injection cell, a pollutant flow rate of 225 L/min has been imposed for both neutral 2681829 and stable 2692157 trials (cf. Table 1). With the Lagrangian approach, at the same injection cell, 2 000 particles per time step have been injected, with the same flow rate.

4.3. Results for neutral trial 2681829

4.3.1. Simulation of the fluid phase

As exposed in the previous section, two simulations of the fluid phase have been performed, corresponding respectively to the use of the $k-\epsilon$ or second-order $R_{ij}-\epsilon$ turbulence closures. Figure 4 shows the mean velocity and TKE fields at height $z = 4$ m for both

turbulence models. This height stands above the roofs ($z_{roofs} = 2.54$ m) and we can observe the influence of the row of containers on the flow. Naturally, a slowdown of the flow and an increase in turbulent kinetic energy can be observed. It can also be seen that $k-\epsilon$ model tends to predict higher levels of turbulent kinetic energy upstream of the obstacles, which is a well-known result in turbulence modeling. However, when comparing to the measurements, it can be seen that the TKE values are always underestimated, with both $k-\epsilon$ and $R_{ij}-\epsilon$ models. Figure 5 shows the wind field in the source area, at 1.6 m height: the recirculation zones between the containers are well-captured and explain the previously mentioned decrease of velocity above the roofs at 4 m height. The recirculation zones are also wider and more pronounced with the $R_{ij}-\epsilon$ model. Finally, the mean velocity and TKE vertical profiles extracted from the masts have been plotted in Figure 6 when data was available. Once again, turbulence production is more pronounced with $k-\epsilon$ model. Velocity profiles are on the other hand not much affected by the turbulence model (as is also seen in the velocity magnitude field of Figure 4) and stand in good agreement with the measurements.

4.3.2. Simulation of the dispersion

Figure 7 shows the concentration fields at height 1.6 m, for both $k-\epsilon$ and $R_{ij}-\epsilon$ models. Whether it be through the Eulerian or the Lagrangian approach, it can be observed that the choice of the turbulence model plays an important role on the concentration patterns. In particular, it can be seen that the plume is wider using the $R_{ij}-\epsilon$ model.

One can also observe that there is a deflection of the plume centerline compared to the -41^o wind direction. Note also that the plume deflection is more pronounced when using the $R_{ij}-\epsilon$ model, for both Eulerian and Lagrangian approaches. This deviation phenomenon has also been observed in Carissimo and Macdonald (2004) and Milliez and Carissimo (2007). Milliez and Carissimo (2007) explained it by the fact the pollutant is channeled into the streets perpendicular to the obstacle array axis, as is also observed in the experiment. Castelli et al. (2017), who also performed the same trial Eulerian $k-\epsilon$ and Lagrangian calculations within their models RAMS6.0-mod and MicroRMS, noticed a lesser pronounced deflection with the Lagrangian modeling. They partly explained it by pointing out that their Lagrangian code did not account for the cross-correlation terms between the different components of wind velocity fluctuations. This is not the case with the model used in the present work since it is based on Pope's SLM, which implies that the cross-correlations of the wind velocity fluctuations are included in the mean-pressure gradient term of Eq. (4b). This is actually one of the main advantages of this formulation, see Bahlali et al. (2018b) for more theoretical details. This may be why, when roughly comparing the concentration field obtained by Castelli et al. (2017) to the one displayed in Figure 7, a more pronounced deflection is found with the SLM than in Castelli et al. (2017)'s results.

For a more precise analysis of the concentration field, the concentration horizontal profiles on lines 1, 2, 3, 4 are shown in Figure 8, and the vertical profiles on masts B, C, D and tower T are displayed in Figure 9. It can be observed that, in particular, the lines 1 and

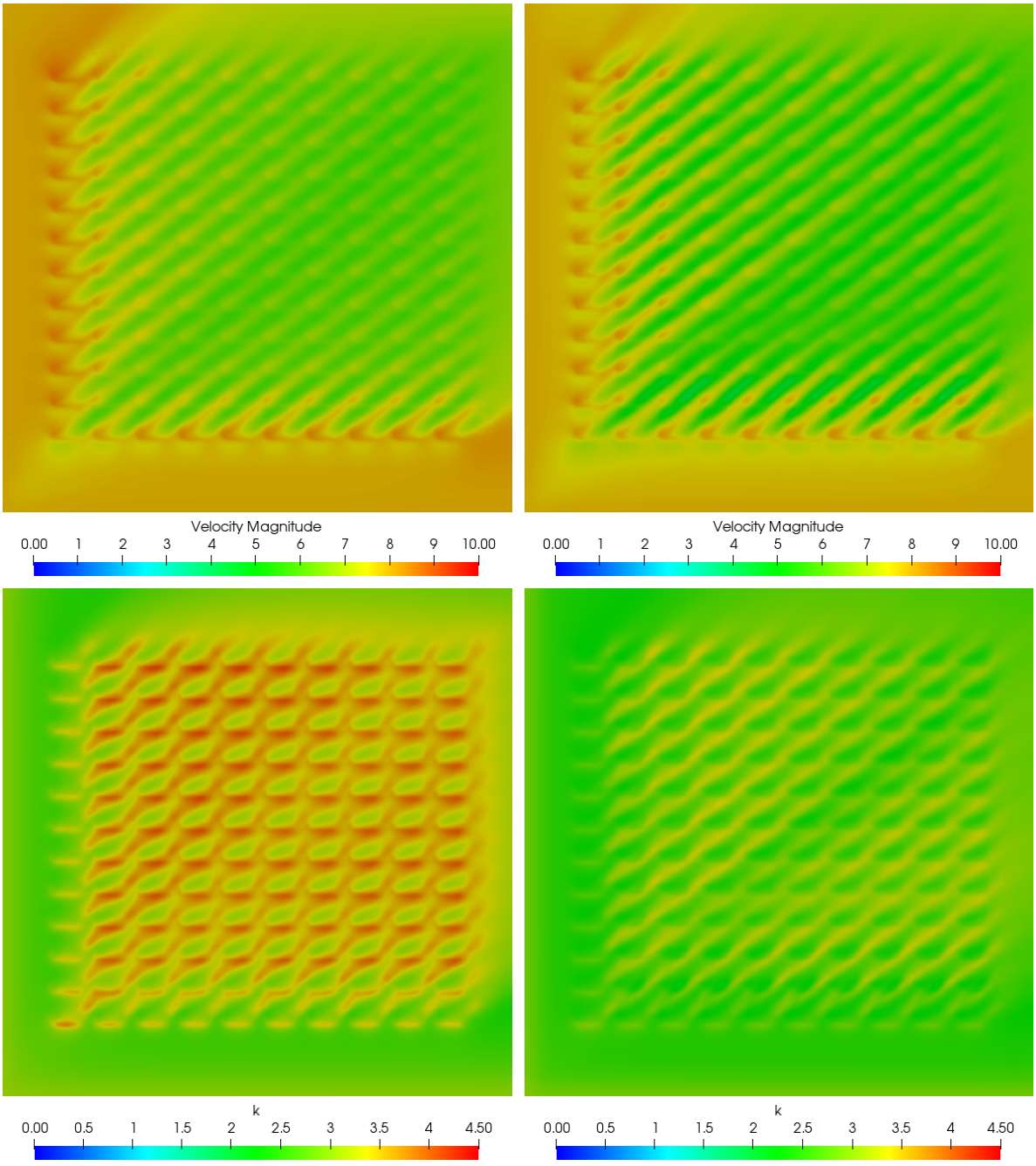

(a) $k - \epsilon$ model (b) $R_{ij} - \epsilon$ model

Figure 4: Comparison of mean velocity and TKE fields at $z = 4$ m computed by $k-\epsilon$ or $R_{ij}-\epsilon$ turbulence models, for neutral trial 2681829.

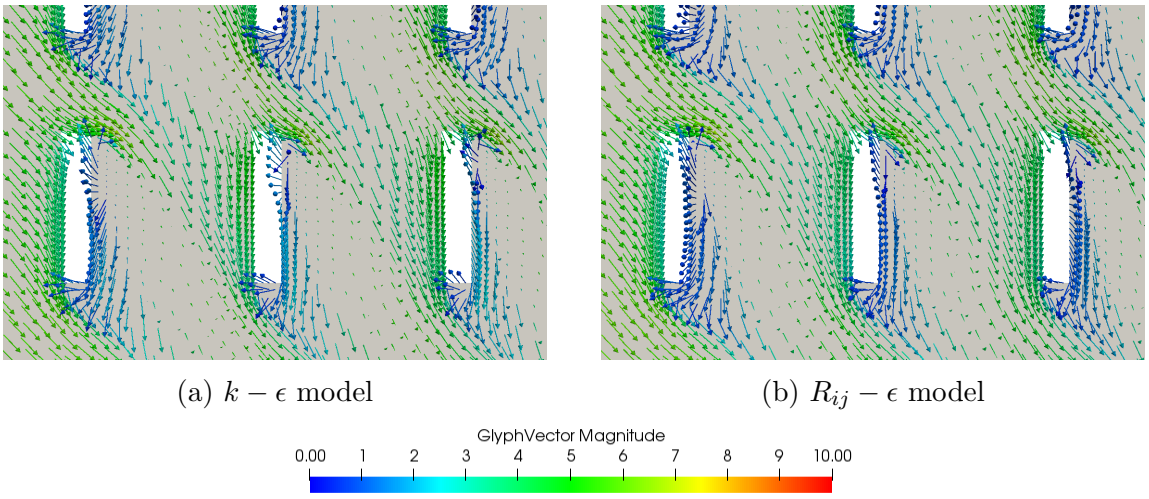

(a) $k-\epsilon$ model (b) $R_{ij}-\epsilon$ model

Figure 5: Comparison of wind fields around the source computed by $k-\epsilon$ or $R_{ij}-\epsilon$ turbulence models, for neutral trial 2681829.

2 show a shift in the plumes obtained by respectively the $k-\epsilon$ and the $R_{ij}-\epsilon$ models, which again highlights the observed more pronounced deflection with the $R_{ij}-\epsilon$ closure. When using the $R_{ij}-\epsilon$ closure, the effect of the obstacles is clearly visible through the 'steps' corresponding to the regular spacing between the containers. If one compares Eulerian to Lagrangian results, it is interesting to have a look at the concentration evolution from line 1 (closest to the source) to line 4. Both models seem to have approximately the same evolution of diffusion. This is better seen in Figure 10, where the maximum concentration value over each line against the distance from the source has been plotted. It is well-known that Langevin-like Lagrangian models show rapid diffusion near the source and then tend to follow the diffusive law in the far-field. On the other hand, Eulerian models based on a simple gradient diffusion hypothesis portray the whole dispersion process by the diffusive law (which is actually a shortcoming of this kind of models since the gradient-diffusion hypothesis is no longer valid near the source). One then might wonder why, here in Figure 10, both Eulerian and Lagrangian models seem to show the same evolution of diffusion, independently from the distance to the source. In fact, one important thing to point out here is that line 1 is already located in the so-called 'far-field region'. Indeed, when speaking about near and far fields, it is always in comparison to the value of the Lagrangian integral timescale T_L. For small diffusion times with respect to the value of T_L, diffusion should be evolving proportionally to time, while for higher diffusion times, it should be evolving as square-root of time (Taylor, 1921). In the present case, the value of T_L at the injection cell is 0.93 s, and the velocity norm is 4.5 m.s^{-1}, which yields a 'near-field region' of approximately $0.93 \times 4.5 = 4.2$ m. The far field is thus quickly reached. As the maximum concentration value on line 1 is located at approximately 60 m ($\gg 4.2$ m) from the source, we deduce by extension that all the lines are already in the well-established far-field region. In consequence, it is only logical that both the Lagrangian and the Eulerian models show the same evolution of diffusion.

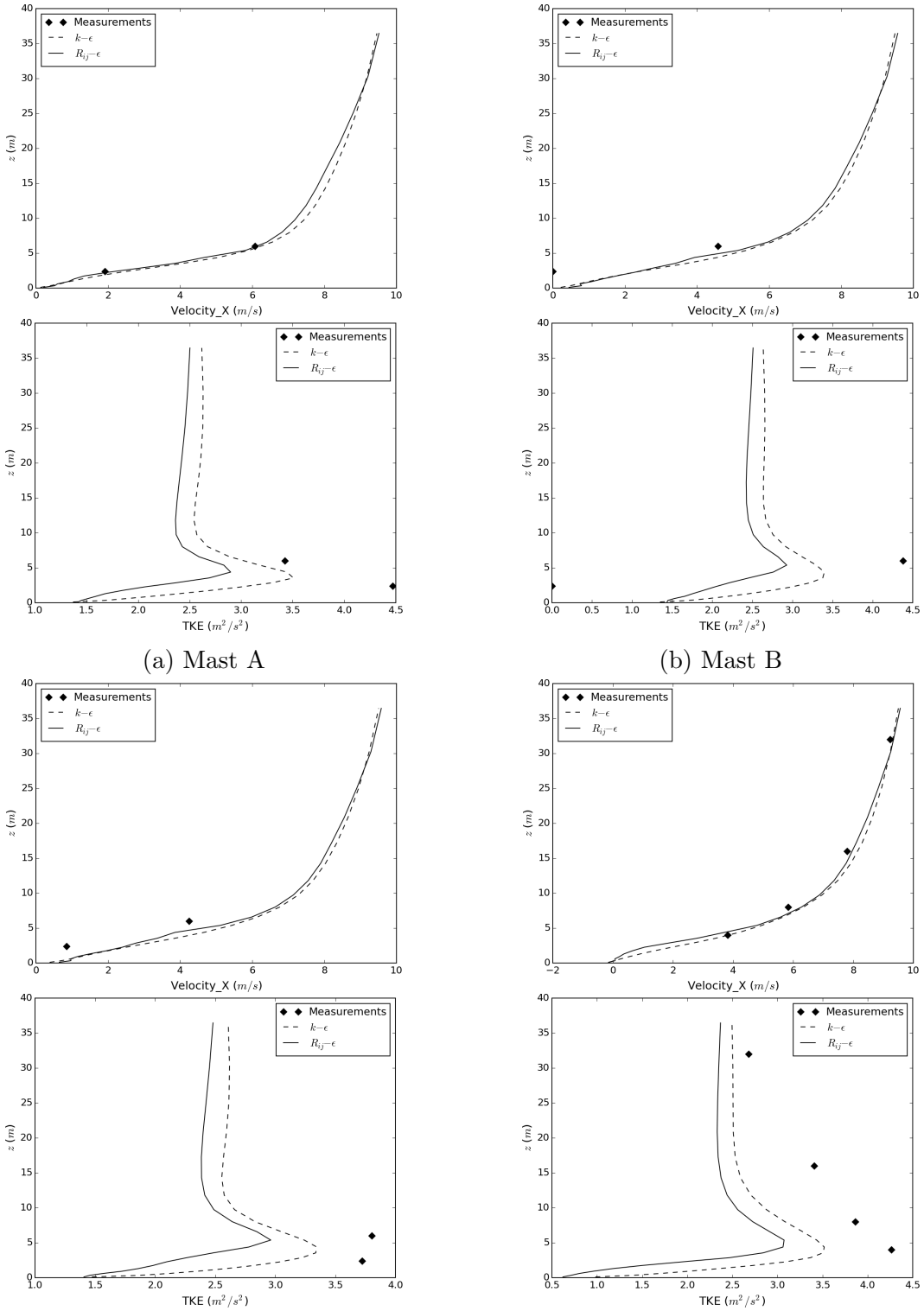

(a) Mast A

(b) Mast B

(c) Mast D

(d) Tower T

Figure 6: Comparison of vertical velocity and TKE profiles computed by $k-\epsilon$ or $R_{ij}-\epsilon$ turbulence models, for neutral trial 2681829.

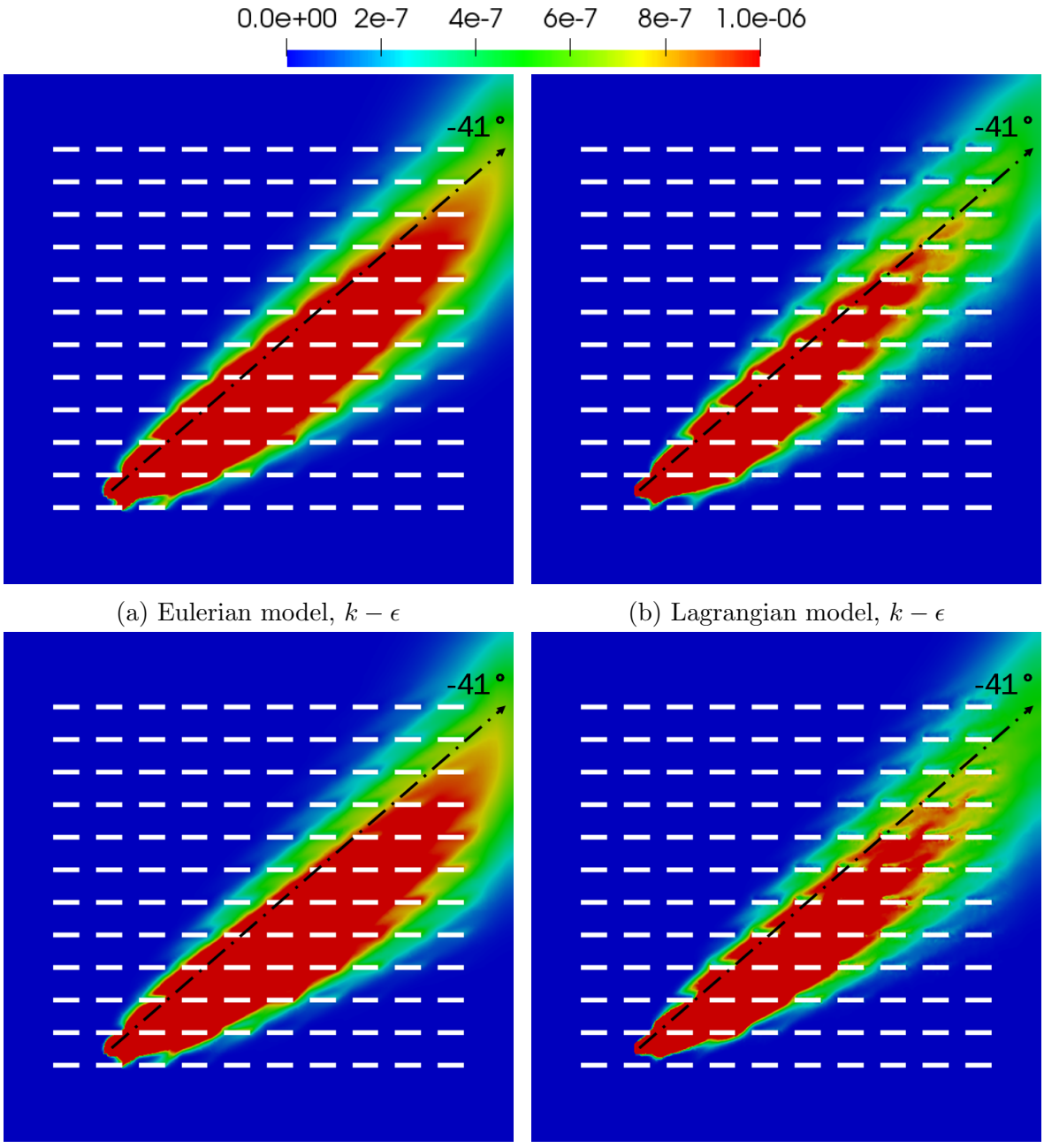

(a) Eulerian model, $k - \epsilon$

(b) Lagrangian model, $k - \epsilon$

(c) Eulerian model, $R_{ij} - \epsilon$

(d) Lagrangian model, $R_{ij} - \epsilon$

Figure 7: Comparison of mean concentration (kg/kg) fields at $z = 1.6$ m computed by both Eulerian and Lagrangian models, through $k - \epsilon$ or $R_{ij} - \epsilon$ turbulence closures, for neutral trial 2681829.

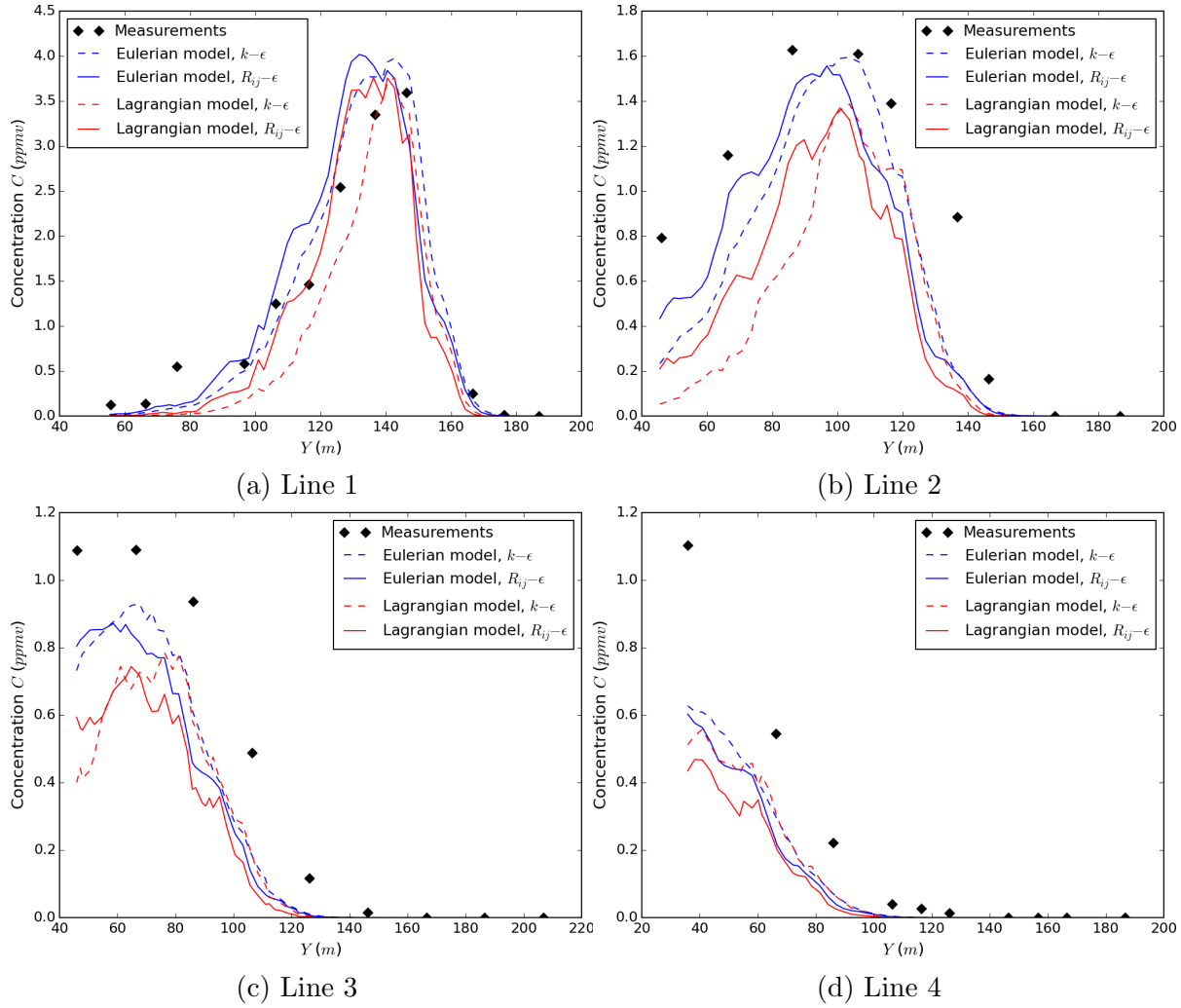

Figure 8: Comparison of concentration profiles on horizontal line samplers computed by both Eulerian and Lagrangian models, through $k-\epsilon$ or $R_{ij}-\epsilon$ turbulence closures, for neutral trial 2681829.

Apart from the previous remarks, and still analyzing the lines, the agreement between simulations and measurements is overall satisfactory and both Eulerian and Lagrangian models provide a quite acceptable representation of the spread of the plume, although the Lagrangian model seems to slightly underestimate the concentrations on all the lines.

If we focus now on vertical profiles (see Figure 9), it can be seen that the use of the $R_{ij}-\epsilon$ model for the fluid phase tends to reduce the maxima of concentrations on mast B (closest to the source), especially with the Lagrangian approach, making the results in better agreement with the measurements. On tower T, the maxima of concentrations are also lower and are due to the fact that the plume deflection is more pronounced using the $R_{ij}-\epsilon$ model for both Eulerian and Lagrangian approaches, making the plume go towards the South direction with more intensity and leaving lower concentration values on tower T. On mast C, the concentrations are also slightly reduced when using the $R_{ij}-\epsilon$ model for

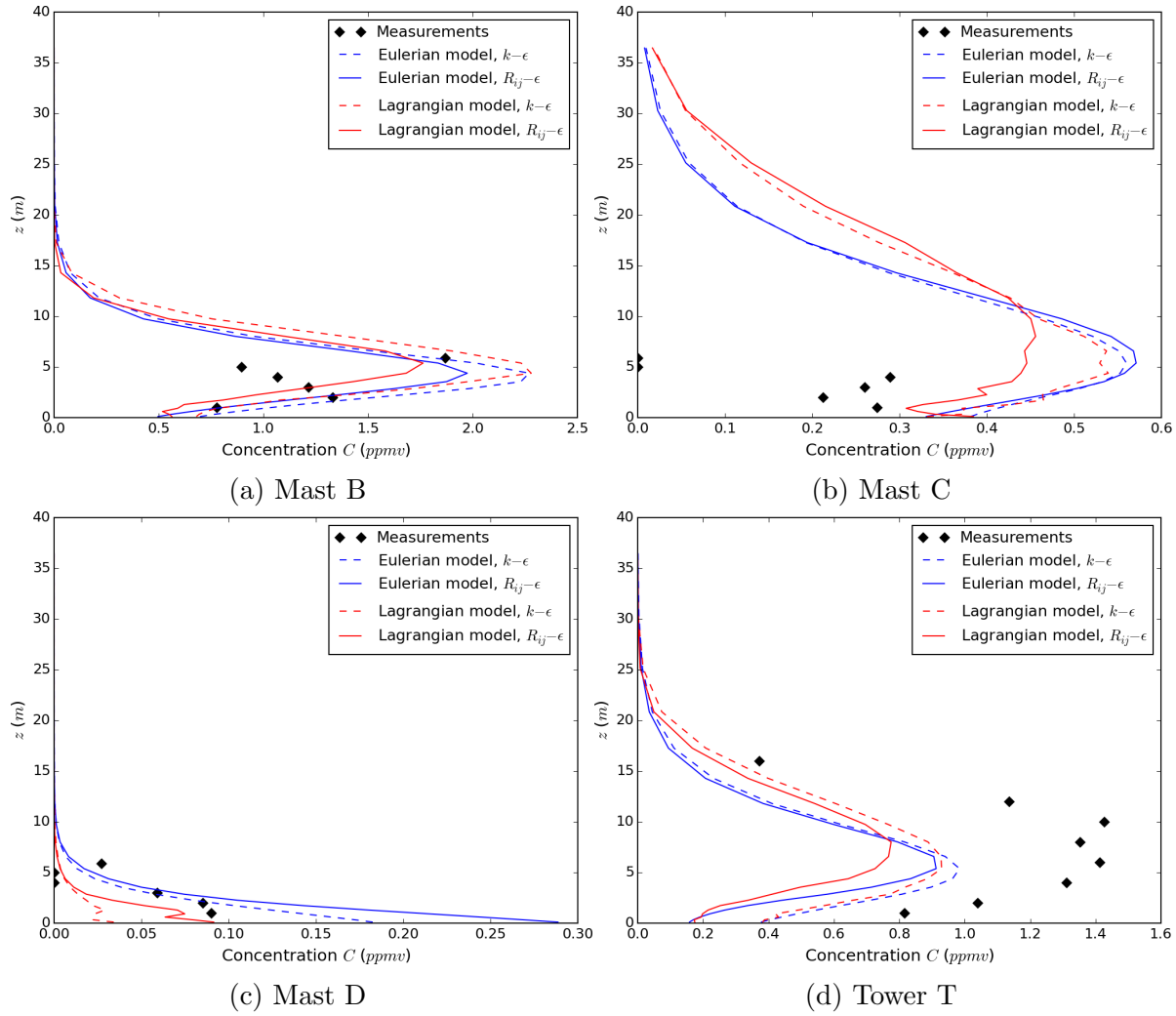

(a) Mast B

(b) Mast C

(c) Mast D

(d) Tower T

Figure 9: Comparison of vertical concentration profiles computed by both Eulerian and Lagrangian models, through $k-\epsilon$ or $R_{ij}-\epsilon$ turbulence closures, for neutral trial 2681829.

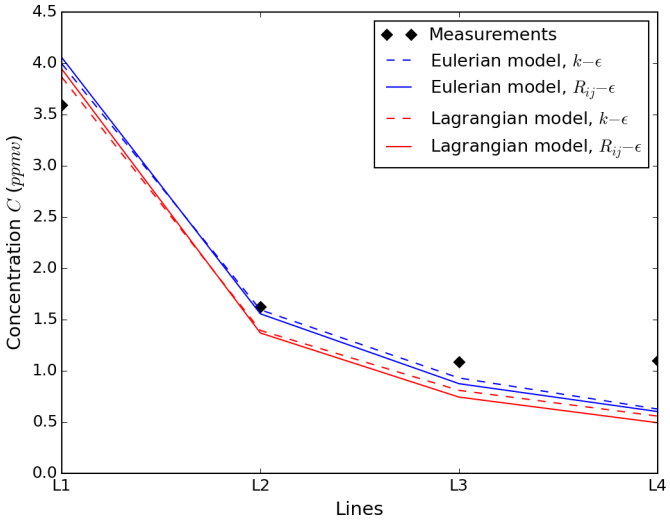

Figure 10: Maximum concentration value over each line against the distance from the source, for neutral trial 2681829.

the same reason as for tower T. It is interesting to note that on this mast, the Lagrangian approach captures the change of sign in the vertical gradient of concentration near the ground, while the Eulerian model does not. This is even more marked with the use of the $R_{ij} - \epsilon$ model. Finally, on mast D, concentrations are raised up when using the $R_{ij} - \epsilon$ model, which can also be explained by the plume deflection towards the South direction more pronounced with this model. On this mast, the Lagrangian approach provides better agreement with the measurements. However, note that one must be cautious in giving definite conclusions for masts C and D, since the concentrations are lower and can then imply more significant errors and uncertainties.

4.4. Results for stable trial 2692157

4.4.1. Simulation of the fluid phase

Analogously to neutral trial 2681829, we show in Figure 11 the mean velocity and TKE vertical profiles on masts A, B, C and tower T for both $k-\epsilon$ and $R_{ij}-\epsilon$ turbulence models. Velocities and TKE values are much lower than for trial 2681829, which is typical of stable stratification meteorological conditions. As in case 2681829, $k-\epsilon$ model tends to predict higher values of TKE than does $R_{ij}-\epsilon$ model. Velocity profiles are in good agreement with the measurements. Once again, they are not much affected by the choice of the turbulence model.

4.4.2. Simulation of the dispersion

Figure 12 displays the different concentration fields at height 1.6 m. It can be seen that as in trial 2681829, the plume is also wider when $R_{ij} - \epsilon$ model is used. The difference is even more pronounced through the Lagrangian approach. In addition, a plume deflection (compared to the 43^o wind direction) can also be observed in both Eulerian and Lagrangian

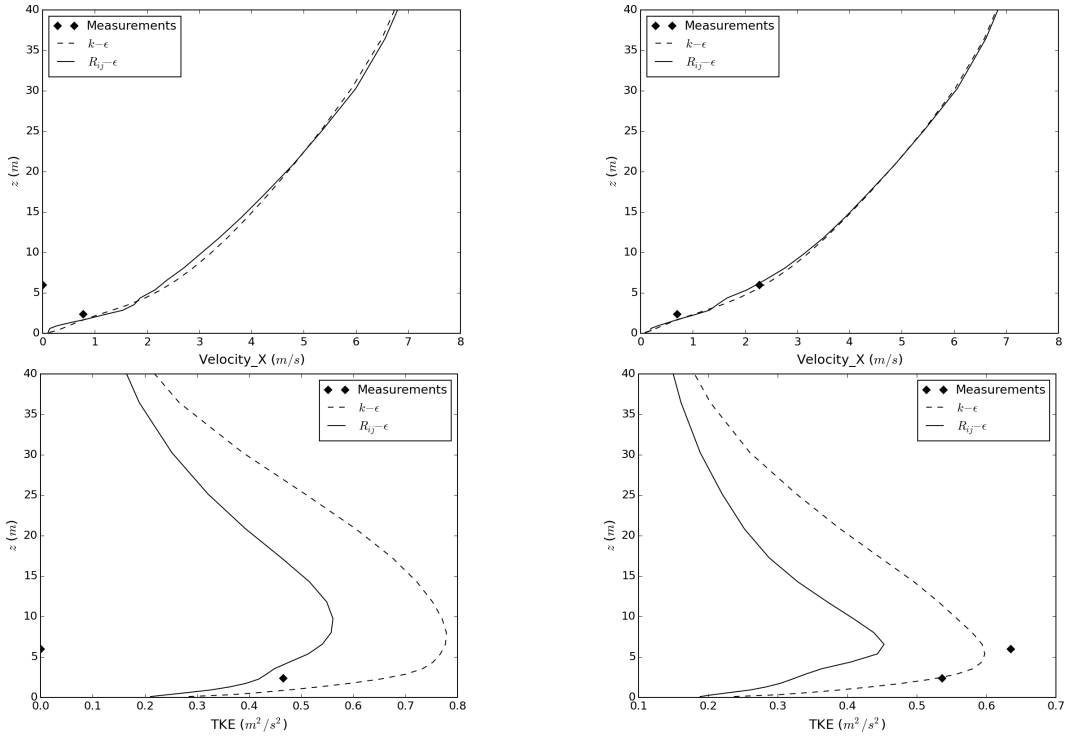

(a) Mast A

(b) Mast B

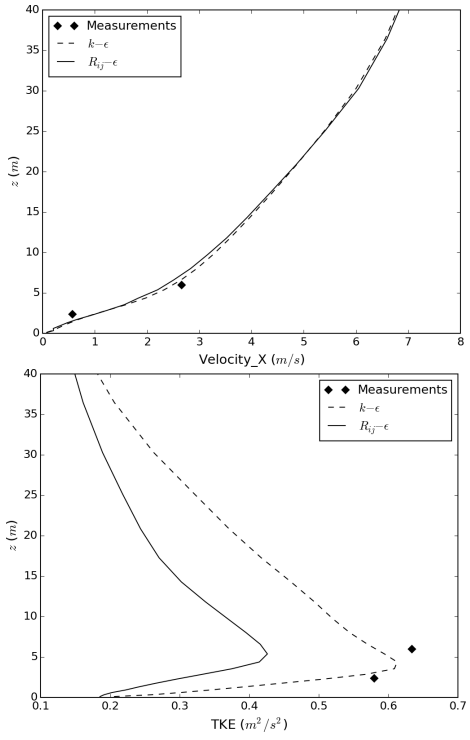

(c) Mast C

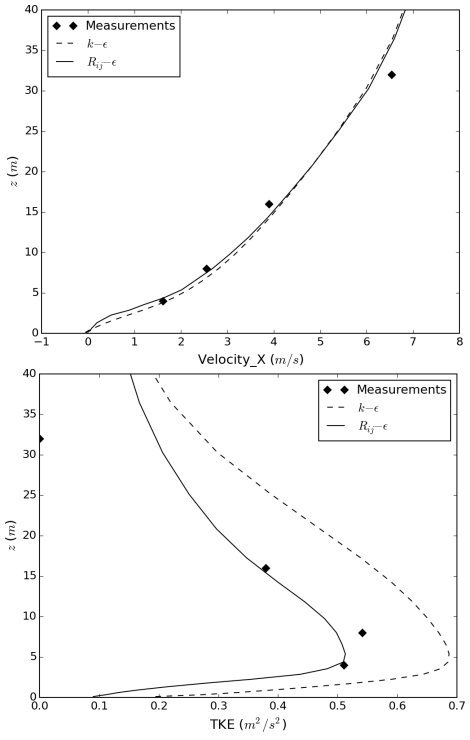

(d) Tower T

Figure 11: Comparison of vertical velocity and TKE profiles computed by $k-\epsilon$ or $R_{ij}-\epsilon$ turbulence models, for stable trial 2692157.

results, more significant when using the $R_{ij} - \epsilon$ than the $k - \epsilon$ model for the fluid phase computation.

The horizontal concentration profiles on lines 1, 2, 3 and 4 are shown in Figure 13. It can be seen that the use of the $R_{ij} - \epsilon$ model leads to an overprediction of concentrations on line 1, for both Eulerian and Lagrangian approaches, even more marked on the Eulerian results. Such an overprediction may be due to the fact that TKE is underestimated with the $R_{ij} - \epsilon$ model as seen in Figure 11. Nevertheless, the $R_{ij} - \epsilon$ model shows again the advantage of better capturing the presence of the obstacles through the visible regular concentration 'steps'. Regardless of the turbulence model, one can also notice the strong decrease of concentrations between line 1 and line 2 with both Lagrangian and Eulerian models, less marked when moving to the next lines: the evolution of diffusion induced by both models look similar. In this trial, at the injection cell, $T_L = 0.73$ s and the velocity equals 1.7 m.s^{-1}: in consequence, the region corresponding to the 'near field' corresponds to distances below $0.73 \times 1.7 = 1.2$ m. The far field is thus immediately reached. Finally, one may notice that the larger the distance from the source, the closer Eulerian and Lagragian curves approach each other. Also, the agreement with experimental measurements is much better.

The vertical concentration profiles on masts A, B, D and tower T are displayed in Figure 14. On mast D, which is the closest to the source, both Lagrangian and Eulerian models overpredict the concentrations when the $R_{ij} - \epsilon$ model is used. Nevertheless, when using the $k - \epsilon$ closure, both models provides very accurate results. Same goes for tower T, where the use of the $R_{ij} - \epsilon$ turbulence closure leads to an overprediction of concentration especially near the ground. On this mast, it is interesting to point out that even though the Lagrangian model used with the $k - \epsilon$ closure underpredicts the concentration values, it captures the change in the sign of the vertical concentration gradient near the ground. Stepping even further from the source and looking at mast A, one can notice a stronger vertical diffusion in the Lagrangian results. In this case again, concentrations are overpredicted. For this trial, the study of masts D, T and A is interesting as the 'D-T-A' parametrical line is roughly aligned with the centerline of the plume. One general conclusion from these three masts is that the use of the $R_{ij} - \epsilon$ model leads to an overprediction of concentrations especially near the ground. As for the concentrations on mast B, they are influenced by the plume deviation. Indeed, since the $R_{ij} - \epsilon$ model involves a more pronounced deflection of the plume than the $k - \epsilon$ model towards the West direction, where mast B is located, then concentrations are expected to be higher, which is indeed what is observed in the simulation results. However, and once again, better accuracy is found when the $k - \epsilon$ model is used for both Eulerian and Lagrangian approaches (except on mast B for the Lagrangian results).

From all these results on stable stratification, one may think that the tendency of the $k - \epsilon$ model to compute high TKE values can be seen as an 'advantage' for stable conditions, since this strengthens diffusion processes and thus leads to lower concentration values (that are, in general, and in particular looking at the lines, in better agreement with the measurements). In fact, one should remember here that even when using a $R_{ij} - \epsilon$

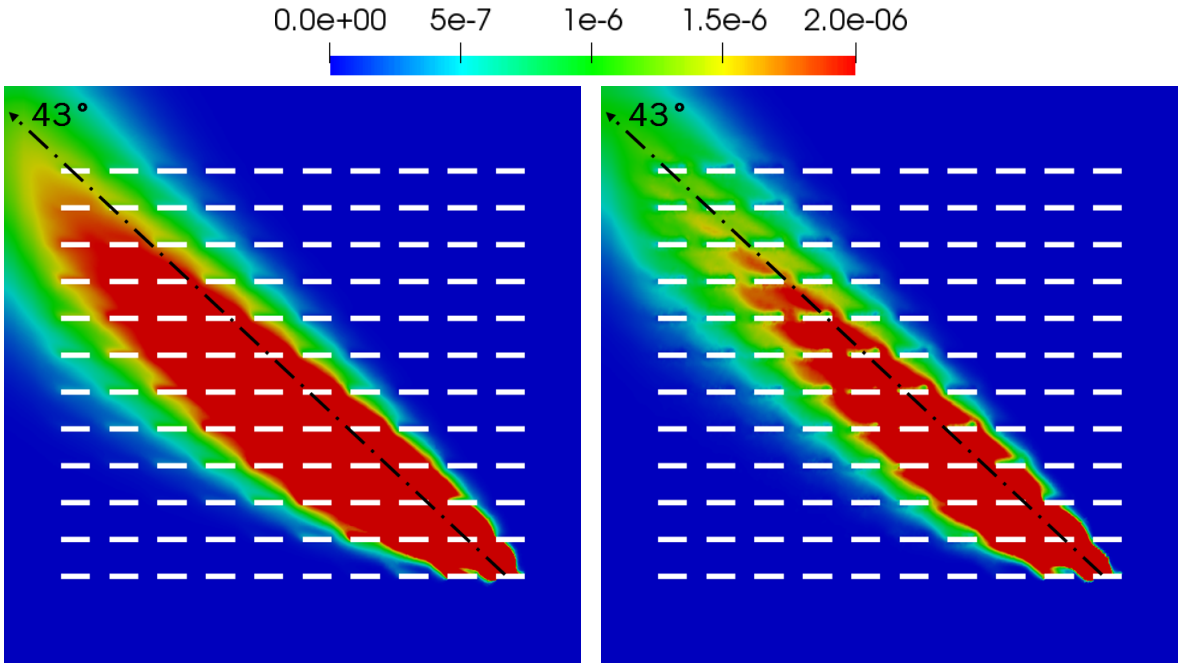

(a) Eulerian model, $k - \epsilon$ (b) Lagrangian model, $k - \epsilon$

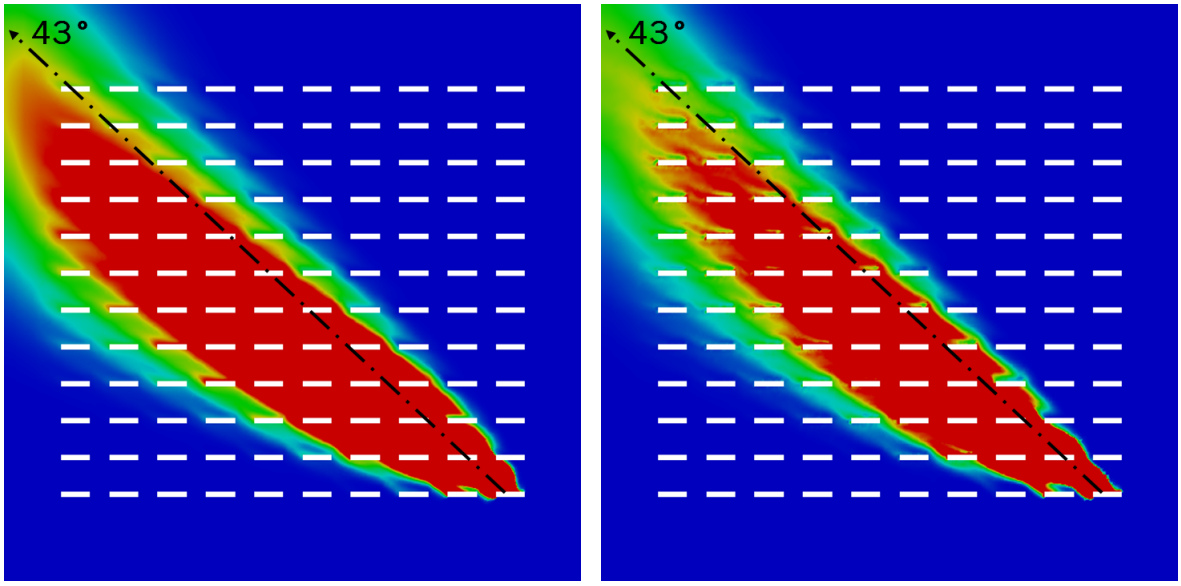

(c) Eulerian model, $R_{ij} - \epsilon$ (d) Lagrangian model, $R_{ij} - \epsilon$

Figure 12: Comparison of mean concentration (kg/kg) fields at $z = 1.6$ m computed by both Eulerian and Lagrangian models, through $k - \epsilon$ or $R_{ij} - \epsilon$ turbulence closures, for stable trial 2692157.

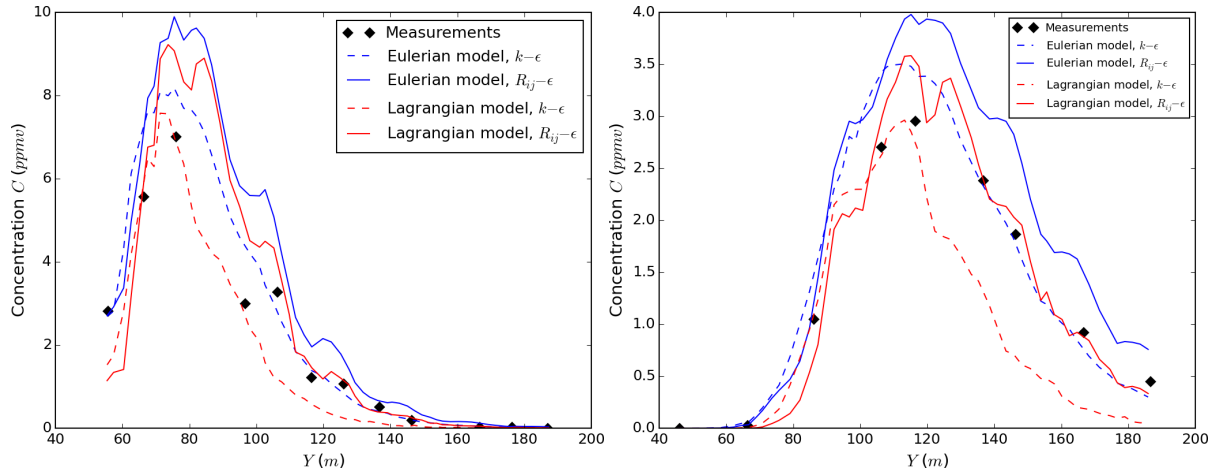

(a) Line 1

(b) Line 2

(c) Line 3

(d) Line 4

Figure 13: Comparison of concentration profiles on horizontal line samplers computed by both Eulerian and Lagrangian models, through $k-\epsilon$ or $R_{ij}-\epsilon$ turbulence closures, for stable trial 2692157.

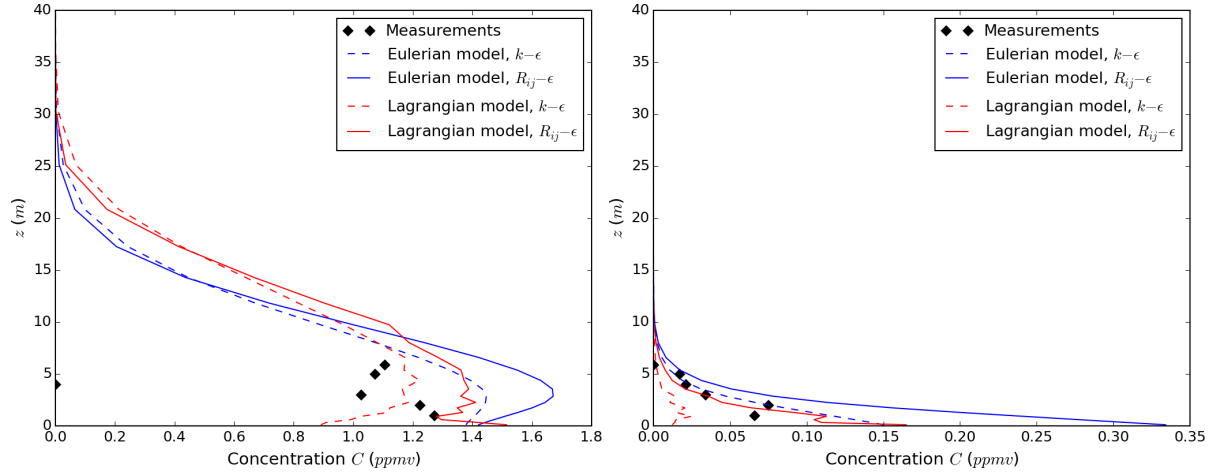

(a) Mast A

(b) Mast B

(c) Mast D

(d) Tower T

Figure 14: Comparison of vertical concentration profiles computed by both Eulerian and Lagrangian models, through $k-\epsilon$ or $R_{ij}-\epsilon$ turbulence closures, for stable trial 2692157.

model, the closure on potential temperature is still local, through the following Generalized Gradient Diffusion Hypothesis (GGDH):

$$\langle U'_{f,j}\theta'\rangle = -C_\theta \frac{k}{\epsilon}\left(\langle U'_{f,j}U'_{f,k}\rangle \frac{\partial\langle\theta\rangle}{\partial x_k}\right) \ , \tag{6}$$

where $C_\theta = 0.3$.

An improvement, still under investigation, could be the use of a second-order model on potential temperature.

5. Conclusions

This work aimed at assessing the ability of a Lagrangian stochastic model to perform point source dispersion in an idealized urban area, for neutral and stable meteorological conditions. The Lagrangian model used was a model based on Pope (2000)'s SLM and Minier and Peirano (2001)'s two-phase flow formulation. Pope's PDF models have gone quite unnoticed in the atmospheric dispersion community, despite presenting some non-negligible theoretical and numerical advantages (see Bahlali et al. (2018a,b)).

As used within a hybrid Eulerian/Lagrangian approach, the Lagrangian solver was fed by the mean dynamical fields provided by the Eulerian solver of the same CFD code *Code_Saturne*. These fields were computed either through a $k-\epsilon$ model or a second-order $R_{ij}-\epsilon$ model. The Lagrangian results were compared to the Eulerian ones, for both turbulence models. The Eulerian turbulence closure for the scalar fluctuations was based on the gradient-diffusion hypothesis, which implied constant diffusivity. We showed that since the region considered for concentration measurements is already located in the far field (*i.e.*, diffusion times higher than the Lagrangian integral timescale), both Eulerian and Lagrangian show the same evolution of diffusion.

Then, we showed that the obstacle array induced a deflection of the plume, as already observed by Milliez and Carissimo (2007) in the same code and Castelli et al. (2017) in another methodology. These works modeled turbulence only through a $k-\epsilon$ closure. More precisely, we showed that this plume deflection was more pronounced using a $R_{ij}-\epsilon$ model. This was the case with both Eulerian and Lagrangian approaches. For neutral stratification, the agreement between results and measurements is quite satisfactory. In particular, we can validate the accuracy of the results of the Lagrangian model. We showed that the use of the $R_{ij}-\epsilon$ model made it possible to have a more physical representation of the obstacles' influence on the concentration profiles, through the visible regular 'steps' corresponding to the spacing between the containers.

For stable stratification, we showed that the results obtained by both approaches were more accurate when using a $k-\epsilon$ closure for the fluid phase. Not as satisfactory results as for neutral trial were found with the use of the $R_{ij}-\epsilon$ closure for stable stratification. The Lagrangian model, which is dependent on the quality of the flow calculated by the Eulerian solver, also see its results affected by the use of the $R_{ij}-\epsilon$ model. Deeper investigations are

needed on this subject, as it should be noted that the temperature and scalar fluctuations closures are still local even when using the $R_{ij} - \epsilon$ model.

It is worth noting that the differences between the various results shown in this paper can be interpreted in different ways. In a practical context where order of magnitude differences are expected, they can be seen as small. On the other hand, they can also be looked at as an estimate we can have on the uncertainty effects of adopting either a certain turbulence closure ($k - \epsilon$ or $R_{ij} - \epsilon$) or one of the two Lagrangian or Eulerian approaches.

For further investigations, an idea would be to explore full second-moment closure modeling for both temperature and scalar fluctuations. In the Lagrangian modeling, another research path would be to add a temperature scalar to the state vector of the particles, driven by a new stochastic differential equation (in the spirit of the works of Das and Durbin (2005) or Bossy et al. (2018) for instance), in order to better account for buoyancy-induced turbulent patterns.

Acknowledgements

The work of M. L. Bahlali was supported by CEREA, a member of the Pierre-Simon Laplace Institute (IPSL).

References

Alessandrini, S., Ferrero, E., 2009. A hybrid Lagrangian–Eulerian particle model for reacting pollutant dispersion in non-homogeneous non-isotropic turbulence. Physica A: Statistical Mechanics and its Applications 388 (8), 1375–1387.

Amicarelli, A., Leuzzi, G., Monti, P., et al., 2012. Lagrangian micromixing models for concentration fluctuations: an overview. American Journal of Environmental Sciences 8 (6), 577–590.

Antonioni, G., Burkhart, S., Burman, J., Dejoan, A., Fusco, A., Gaasbeek, R., Gjesdal, T., Jäppinen, A., Riikonen, K., Morra, P., et al., 2012. Comparison of CFD and operational dispersion models in an urban-like environment. Atmospheric Environment 47, 365–372.

Archambeau, F., Méchitoua, N., Sakiz, M., 2004. Code Saturne: A finite volume code for the computation of turbulent incompressible flows-Industrial applications. International Journal on Finite Volumes 1 (1), http://code–saturne.org.

Bahlali, M. L., Dupont, E., Carissimo, B., 2018a. A hybrid CFD RANS/Lagrangian approach to model atmospheric dispersion of pollutants in complex urban geometries. International Journal of Environment and Pollution 64 (1-3), 74–89.

Bahlali, M. L., Henry, C., Carissimo, B., 2018b. On the well-mixed condition and consistency issues in hybrid Eulerian/Lagrangian stochastic models of dispersion. Submitted to Boundary-Layer Meteorology.

Bernardin, F., Bossy, M., Chauvin, C., Drobinski, P., Rousseau, A., Salameh, T., 2009. Stochastic downscaling method: application to wind refinement. Stochastic Environmental Research and Risk Assessment 23 (6), 851–859.

Biltoft, C. A., 2001. Customer report for Mock Urban Setting Test. DPG Document Number 8-CO-160-000-052. Prepared for the Defence Threat Reduction Agency.

Blocken, B., 2014. 50 years of computational wind engineering: past, present and future. Journal of Wind Engineering and Industrial Aerodynamics 129, 69–102.

Blocken, B., Stathopoulos, T., 2013. CFD simulation of pedestrian-level wind conditions around buildings: Past achievements and prospects. Journal of Wind Engineering and Industrial Aerodynamics 121, 138–145.

Bossy, M., Dupré, A., Drobinski, P., Violeau, L., Briard, C., 2018. Stochastic Lagrangian approach for wind farm simulation, http://hal.inria.fr/hal–01697815/.

Camelli, F., Lohner, R., Hanna, S., 2005. VLES study of MUST experiment. In: 43rd AIAA Aerospace Sciences Meeting and Exhibit. p. 1279.

564 Carissimo, B., Macdonald, R., 2004. A porosity/drag approach for the modeling of flow
565 and dispersion in the urban canopy. In: Air Pollution Modeling and Its Application XV.
566 Springer, pp. 385–393.

567 Cassiani, M., Franzese, P., Giostra, U., 2005a. A PDF micromixing model of dispersion
568 for atmospheric flow. Part I: development of the model, application to homogeneous
569 turbulence and to neutral boundary layer. Atmospheric Environment 39 (8), 1457–1469.

570 Cassiani, M., Franzese, P., Giostra, U., 2005b. A PDF micromixing model of dispersion
571 for atmospheric flow. Part II: application to convective boundary layer. Atmospheric
572 Environment 39 (8), 1471–1479.

573 Cassiani, M., Stohl, A., Brioude, J., 2015. Lagrangian Stochastic Modelling of Disper-
574 sion in the Convective Boundary Layer with Skewed Turbulence Conditions and a Ver-
575 tical Density Gradient: Formulation and Implementation in the FLEXPART Model.
576 Boundary-Layer Meteorology 154 (3), 367–390.

577 Castelli, S. T., Tinarelli, G., Reisin, T., 2017. Comparison of atmospheric modelling sys-
578 tems simulating the flow, turbulence and dispersion at the microscale within obstacles.
579 Environmental Fluid Mechanics 17 (5), 879–901.

580 Das, S., Durbin, P. A., 2005. A Lagrangian stochastic model for dispersion in stratified
581 turbulence. Physics of Fluids 17 (2), 025109.

582 Dejoan, A., Santiago, J., Martilli, A., Martin, F., Pinelli, A., 2010. Comparison be-
583 tween Large-Eddy Simulation and Reynolds-averaged Navier–Stokes computations for
584 the MUST field experiment. Part II: effects of incident wind angle deviation on the
585 mean flow and plume dispersion. Boundary-Layer Meteorology 135 (1), 133–150.

586 Donnelly, R., Lyons, T., Flassak, T., 2009. Evaluation of results of a numerical simulation
587 of dispersion in an idealised urban area for emergency response modelling. Atmospheric
588 Environment 43 (29), 4416–4423.

589 Duynkerke, P., 1988. Application of the E–ε turbulence closure model to the neutral and
590 stable atmospheric boundary layer. Journal of the Atmospheric Sciences 45 (5), 865–880.

591 Franke, J., Hirsch, C., Jensen, A., Krüs, H., Schatzmann, M., Westbury, P., Miles, S.,
592 Wisse, J., Wright, N., 2004. Recommendations on the use of CFD in wind engineering.
593 In: COST action C. Vol. 14. p. C1.

594 Franzese, P., 2003. Lagrangian stochastic modeling of a fluctuating plume in the convective
595 boundary layer. Atmospheric Environment 37 (12), 1691–1701.

596 Gardiner, C. W., 1985. Handbook of stochastic methods for physics, chemistry and the
597 natural sciences. Springer.

598 Hanna, S. R., Hansen, O. R., Dharmavaram, S., 2004. FLACS CFD air quality model
599 performance evaluation with Kit Fox, MUST, Prairie Grass, and EMU observations.
600 Atmospheric Environment 38 (28), 4675–4687.

601 Kumar, P., Feiz, A.-A., Ngae, P., Singh, S. K., Issartel, J.-P., 2015. CFD simulation of
602 short-range plume dispersion from a point release in an urban like environment. Atmo-
603 spheric Environment 122, 645–656.

604 Leitl, B., Bezpalcova, K., Harms, F., 2007. Wind tunnel modelling of the MUST experi-
605 ment. In: Proceeding of the 11th International Conference on Harmonization within At-
606 mospheric Dispersion Modelling for Regulatory Purposes, Cambridge. Vol. 2. p. 435e439.

607 Luhar, A. K., Sawford, B. L., 2005. Micromixing modelling of concentration fluctuations
608 in inhomogeneous turbulence in the convective boundary layer. Boundary-Layer Meteo-
609 rology 114 (1), 1–30.

610 Milliez, M., 2006. Modélisation micro-météorologique en milieu urbain: dispersion des
611 polluants et prise en compte des effets radiatifs. Ph.D. thesis, École nationale des ponts
612 et chaussées (France).

613 Milliez, M., Carissimo, B., 2007. Numerical simulations of pollutant dispersion in an ide-
614 alized urban area, for different meteorological conditions. Boundary-Layer Meteorology
615 122 (2), 321–342.

616 Milliez, M., Carissimo, B., 2008. Computational fluid dynamical modelling of concentration
617 fluctuations in an idealized urban area. Boundary-Layer Meteorology 127 (2), 241–259.

618 Minier, J.-P., 2015. On Lagrangian stochastic methods for turbulent polydisperse two-phase
619 reactive flows. Progress in Energy and Combustion Science 50, 1–62.

620 Minier, J.-P., 2016. Statistical descriptions of polydisperse turbulent two-phase flows.
621 Physics Reports 665, 1–122.

622 Minier, J.-P., Chibbaro, S., Pope, S. B., 2014. Guidelines for the formulation of Lagrangian
623 stochastic models for particle simulations of single-phase and dispersed two-phase tur-
624 bulent flows. Physics of Fluids (1994-present) 26 (11), 113303.

625 Minier, J.-P., Peirano, E., 2001. The PDF approach to turbulent polydispersed two-phase
626 flows. Physics Reports 352 (1), 1–214.

627 Mochida, A., Tabata, Y., Iwata, T., Yoshino, H., 2008. Examining tree canopy models for
628 CFD prediction of wind environment at pedestrian level. Journal of Wind Engineering
629 and Industrial Aerodynamics 96 (10-11), 1667–1677.

630 Öttinger, H. C., 1996. Stochastic processes in polymeric fluids: tools and examples for
631 developing simulation algorithms. Springer.

Pope, S., 1998. The vanishing effect of molecular diffusivity on turbulent dispersion: implications for turbulent mixing and the scalar flux. Journal of Fluid Mechanics 359, 299–312.

Pope, S. B., 2000. Turbulent flows.

Salim, S. M., Buccolieri, R., Chan, A., Di Sabatino, S., 2011. Numerical simulation of atmospheric pollutant dispersion in an urban street canyon: Comparison between RANS and LES. Journal of Wind Engineering and Industrial Aerodynamics 99 (2-3), 103–113.

Santiago, J., Dejoan, A., Martilli, A., Martin, F., Pinelli, A., 2010. Comparison between Large-Eddy Simulation and Reynolds-averaged Navier–Stokes computations for the MUST field experiment. Part I: study of the flow for an incident wind directed perpendicularly to the front array of containers. Boundary-Layer Meteorology 135 (1), 109–132.

Sawford, B., 2004. Micro-mixing modelling of scalar fluctuations for plumes in homogeneous turbulence. Flow, Turbulence and Combustion 72 (2-4), 133–160.

Stohl, A., Forster, C., Frank, A., Seibert, P., Wotawa, G., 2005. The Lagrangian particle dispersion model FLEXPART version 6.2. Atmospheric Chemistry and Physics 5 (9), 2461–2474.

Stull, R. B., 1988. An introduction to boundary layer meteorology. Vol. 13. Springer Science & Business Media.

Taylor, G. I., 1921. Diffusion by continuous movements. Proceedings of the London Mathematical Society 20, 196–211.

Thomson, D., 1987. Criteria for the selection of stochastic models of particle trajectories in turbulent flows. Journal of Fluid Mechanics 180, 529–556.

Tinarelli, G., Mortarini, L., Castelli, S. T., Carlino, G., Moussafir, J., Olry, C., Armand, P., Anfossi, D., 2013. Review and validation of MicroSpray, a Lagrangian particle model of turbulent dispersion. Lagrangian Modeling of the Atmosphere, 311–328.

Tominaga, Y., Mochida, A., Yoshie, R., Kataoka, H., Nozu, T., Yoshikawa, M., Shirasawa, T., 2008. AIJ guidelines for practical applications of CFD to pedestrian wind environment around buildings. Journal of Wind Engineering and Industrial Aerodynamics 96 (10-11), 1749–1761.

Tominaga, Y., Stathopoulos, T., 2011. CFD modeling of pollution dispersion in a street canyon: Comparison between LES and RANS. Journal of Wind Engineering and Industrial Aerodynamics 99 (4), 340–348.

Villermaux, J., Devillon, J., 1972. Représentation de la coalescence et de la redispersion des domaines de ségrégation dans un fluide par un modele dinteraction phénoménologique. In: Proceedings of the 2nd International Symposium on Chemical Reaction Engineering. Vol. 26. Elsevier New York, pp. 1–13.

Yee, E., Biltoft, C. A., 2004. Concentration fluctuation measurements in a plume dispersing through a regular array of obstacles. Boundary-Layer Meteorology 111 (3), 363–415.

Yee, E., Gailis, R. M., Hill, A., Hilderman, T., Kiel, D., 2006. Comparison of wind-tunnel and water-channel simulations of plume dispersion through a large array of obstacles with a scaled field experiment. Boundary-Layer Meteorology 121 (3), 389–432.

Yoshie, R., Jiang, G., Shirasawa, T., Chung, J., 2011. CFD simulations of gas dispersion around high-rise building in non-isothermal boundary layer. Journal of Wind Engineering and Industrial Aerodynamics 99 (4), 279–288.

Yoshie, R., Mochida, A., Tominaga, Y., Kataoka, H., Harimoto, K., Nozu, T., Shirasawa, T., 2007. Cooperative project for CFD prediction of pedestrian wind environment in the Architectural Institute of Japan. Journal of Wind Engineering and Industrial Aerodynamics 95 (9-11), 1551–1578.